IIS:0379-301X

UNIVERSITE LIBRE DE BRUXELLES - VRIJE UNIVERSITEIT BRUSSEL

INTER-UNIVERSITY INSTITUTE FOR HIGH ENERGIES

FACTORIAL MOMENTS AND CORRELATIONS IN MESON-NUCLEUS INTERACTIONS AT 250 GeV/c

NA22 Collaboration

Universities of Brussels (ULB-VUB)
Pleinlaan 2
1050 Brussels

May 1990
IIHE-90.03

FACTORIAL MOMENTS AND CORRELATIONS IN MESON–NUCLEUS INTERACTIONS AT 250 GeV/c

EHS–NA22 Collaboration

F. BOTTERWECK[a], M. CHARLET[b,1], P.V. CHLIAPNIKOV[c], A. DE ROECK[b,2], E.A. DE WOLF[b,3], K. DZIUNIKOWSKA[d], A.M.F. ENDLER[e], A. ESKREYS[d], V.G. GAVRJUSEV[f], R.S. HAKOBYAN[g], T. HAUPT[a,4] J.K. KARAMYAN[g], K. KALEBA[d], D. KISIELEWSKA[d], W. KITTEL[a], B.B. LEVCHENKO[f], A.B. MICHALOWSKA[b], K. OLKIEWICZ[d], E.S. SHABALINA[f], O.G. TCHIKILEV[c], V.A. UVAROV[c], F. VERBEURE[b], R. WISCHNEWSKI[h]

Abstract

A sample of 8000 interactions of 250 GeV/c π^+ and K^+ mesons on Al and Au nuclei, is used to search for intermittency effects by calculating the normalized factorial moments of order two to four. No significant effect is observed in the higher moments. Two-body rapidity correlations and Bose-Einstein correlations in these interactions are presented.

[a]University of Nijmegen and NIKHEF-H, NL-6525 ED Nijmegen, The Netherlands

[b]Dept. of Physics, Universitaire Instelling Antwerpen, B-2610 Wilrijk, and Interuniversity Institute for High Energies, B-1050 Brussels, Belgium

[c]Institute for High Energy Physics, SU-142284 Serpukhov, USSR

[d]Institute of Physics and Nuclear Techniques of the Academy of Mining and Metallurgy and Institute of Nuclear Physics, PL-30055 Krakow, Poland; partially supported by grants from CPBP 01.06 and 01.09

[e]Centro Brasileiro de Pesquisas Fisicas, BR-22290 Rio de Janeiro, Brazil

[f]Moscow State University, SU-119899 Moscow, USSR

[g]Institute of Physics, SU-375036 Yerevan, USSR

[h]Institut für Hochenergiephysik, D-O-1615 Berlin-Zeuthen, Germany

[1]EEC Guest Scientist

[2]Onderzoeker IIKW, Brussels, Belgium, now at MPI, München

[3]Bevoegdverklaard Navorser NFWO, Belgium

[4]Now at Syracuse University, Syracuse NY 13244–1130

1 Introduction

The possibility that particle production in multihadron final states may exhibit so-called "intermittent" behaviour was first put forward by Białas and Peschanski [1,2,3]. They suggested to study the normalized factorial moments

$$< F_i >=< n(n-1)\ldots(n-i+1) > / < n^i > \qquad (1)$$

of the multiplicity distribution, and in particular the dependence of these moments on δy, a rapidity interval of decreasing size. Intermittency is observed when the factorial moments exhibit a power law behaviour

$$< F_i > \sim (\delta y)^{-f_i} \qquad \text{with} \qquad f_i > 0. \qquad (2)$$

Intermittent behaviour of particle production is now claimed in all studied types of interactions, such as e^+e^-, $h-h$, $h-A$ and $A-A$ interactions (for recent reviews see ref. [4]) and recently in $\mu - p$ interactions [5].

Moreover, it is remarked that the effect seems to decrease with increasing complexity of the collision partners and with increasing complexity of the final state (larger multiplicity) [4].

From the phenomenological point of view, attempts have been made to understand the experimental observations in various models, such as random cascade models [2], jet models with a selfsimilar branching structure [6], short-range correlation [7], clan structure [8] and Bose-Einstein correlations [9,10]. Recently, a lot of attention has been paid to the connection between the δy behaviour of the factorial moments on one hand and the negative binomial distribution, which describes well the particle multiplicity distributions, and the two-body rapidity correlations on the other hand [7b,9,11].

In this work, we will search for intermittency effects in 250 GeV/c π^+ and K^+ collisions with Al and Au nuclei and study the two-body rapidity correlations. Section 2 is devoted to a short description of the experimental aspects of the data. Results on factorial moments are presented in Sect. 3 and on rapidity correlations in Sect. 4. Bose-Einstein correlations are studied in Sect. 5 and a summary is given in Sect. 6.

2 Experimental data

The results presented here, are obtained with the European Hybrid Spectrometer (EHS), irradiated by a beam of π^+ and K^+ mesons of 250 GeV/c momentum. An Al and a Au foil are inserted in the rapid cycling bubble chamber (RCBC), which serves as track detector with 4π angular acceptance for all interactions in the foils. The experimental set-up, the minimum bias trigger and the selection criteria for the nuclear interactions, are described in more detail in [12,13]. The selection criteria aim

at isolating a set of well measured and reconstructed inelastic interactions in either the Al or the Au target, thereby eliminating both quasi-elastic and coherent interactions. Based on the same sample of events, results have previously been presented on multiplicity distributions [13,14] and on inclusive charged particle distributions [15].

The major features of the detector, used in this work, are:

- the up- and downstream wire and drift chambers, as well as the multicell device ISIS, for the measurement of charged particle tracks,
- the H_2 bubble chamber which allows a precise determination of the charge multiplicity, as well as a measurement of all tracks and identification of slow particles.

The events are selected on the basis of the following criteria:

- the incident particle is well measured in the bubble chamber and its track matches with hits in the upstream wire chamber;
- the reconstructed vertex position is within one of the nuclear targets;
- the outgoing tracks are satisfactorily measured with an error on the momentum $\Delta p/p < 0.25$, the allowed momentum error is restricted to $\Delta p/p < 0.04$ for the study of Bose-Einstein correlations; the accepted loss of tracks, due to measurement or reconstruction problems, is at most one for charge multiplicity up to 10, and at most 20% for higher multiplicities.

Electrons and positrons are identified up to $p_{\rm lab} \simeq 200$ MeV/c and protons up to $p_{\rm lab} \simeq 1.2$ GeV/c, by visual inspection of their ionization in the hydrogen of RCBC. These particles are not used in the subsequent analysis. Among the accepted charged tracks remains a small admixture of unidentified electrons and positrons from γ-conversions in the foils. This admixture is estimated to be smaller than 2% in the Al and smaller than 7% in the Au sample. Since no statistically significant difference is observed for π^+ and K^+ induced interactions, we use the combined sample of π^+ and K^+ collisions with 4200 interactions on Al and 3700 on Au. The combined sample is denoted as M^+Al and M^+Au.

The rapidity $y = \frac{1}{2}\ln(E + p_{||})/(E - p_{||})$ is calculated in the c.m. frame of the meson-nucleon system, i.e. $y = y_{\rm lab} - y_0$ where $y_0 = 3.14$, both for the π^+ and the K^+ beam.

In order to search for intermittency effects, factorial moments must be calculated in small rapidity intervals δy, down to approximately the resolution in y. We therefore show in Fig. 1a–d the average errors on y for positive and for negative particles, in both the Al and Au samples. The average error varies between 0.005 and 0.05, being largest in the central region, due to tracks of a few tens of GeV which are

reconstructed in the first lever arm of the spectrometer, but do not reach the second lever arm (see also Fig. 2.8 of [12b]). The average error on the rapidity difference between two particles is always smaller than 0.07, allowing us to use intervals of δy down to $\delta y \simeq 0.1$.

3 Factorial moments

Different definitions of scaled factorial moments are used in the recent literature. We adopt the two that are most commonly used.
The horizontal averaged scaled factorial moment of order i is defined as

$$< F_i >_H = \frac{1}{< \overline{n}_m >^i} \left\langle \frac{1}{M} \sum_{m=1}^{M} n_m(n_m - 1)\dots(n_m - i + 1) \right\rangle \qquad (4a)$$

with

$$< \overline{n}_m > = \left\langle \frac{1}{M} \sum_{m=1}^{M} n_m \right\rangle \qquad (5)$$

and the vertical averaged scaled factorial moment of order i as

$$< F_i >_V = \frac{1}{M} \sum_{m=1}^{M} \frac{\langle n_m(n_m - 1)\dots(n_m - i + 1)\rangle}{\langle n_m \rangle^i} \qquad (4b)$$

whereby the considered rapidity interval Y is subdivided in M equal subintervals, each of size $\delta y = Y/M$. The multiplicity is n_m in bin m ($m = 1 \dots M$) and the averages $<>$ are taken over all events in the sample. The first definition is also used for $\pi^+/K^+ - p$ interactions at 250 GeV/c obtained in the same experiment and with the same measurement and reconstruction procedures [16]. If non-statistical, self similar fluctuations of many different sizes exist, the δy dependence of the factorial moments is expected [1,2] to exhibit the power law behaviour (2), or equivalently

$$< F_i > \sim \left(\frac{Y}{\delta y}\right)^{f_i} \qquad \text{with} \qquad f_i > 0 \qquad (6)$$

in the limit $\delta y \to 0$. Such behavior shows up as a linear rise of $\ln < F_i >$ versus $-\ln \delta y$. A rapidity interval Y of 3 units ($-2 < y < 1$) is used, where the density of particles is almost constant[1] [15].

Tables 1a–1d and Fig. 2 show the factorial moments of order 2 to 4 for the M^+Al (Fig. 2a for horizontal, 2c for vertical averaging) and M^+Au events (Fig. 2b horizontal, 2d vertical averaging) as a function of the size δy of the subintervals. From this figure it is clear that the slope of $\ln F_i$ versus $-\ln \delta y$ varies continously

[1] If the density dn/dy varies, a correction factor should be introduced [17]. The result of this correction factor in μp interactions is a reduction of the slopes f_i [5]

with the latter quantity, until $-\ln \delta y \approx 0.7$. We therefore fit the slopes in the interval $0.9 < -\ln \delta y < 2.2$ ($0.4 > \delta y > 0.1$). The results of the fits are collected in Table 2 and given as full lines on Fig. 2. All fits are of excellent quality with χ^2/NDF values considerably less than one. The fitted slopes are small in all cases and are even negative for the fourth order. For comparison, we also show in Table 2 the fitted slopes for samples of Monte Carlo events with 20000 events per channel, generated according to the FRITIOF model (version 3.0) [18], and subjected to the same cuts as the experimental data (e.g. protons up to $p_{\rm lab} = 1.2$ GeV/c are excluded from the sample, otherwise the pion mass is assigned). In all cases the slopes obtained from the Monte Carlo events are small. The factorial moments obtained with the FRITIOF events are shown on Fig. 2 as dash-dotted curves. The predicted values for the moments in M^+Al interactions agree quite well with the experimental ones, both for horizontal and vertical averaging, but the discrepancy is large for the Au nucleus.

Bushbeck and Lipa [19a] and Białas [19b] have noted that the slope parameter f_2 decreases with increasing rapidity density dn/dy. Fig. 3 shows this dependence (Fig. 12 from [19b]) for proton-emulsion interactions. Our results on M^+Al and M^+Au collisions with horizontal averaging are also plotted on Fig. 3 and confirm the above behaviour.

In order to re-create the conditions of [20], we limited the sample to events with charge multiplicity at least 10 and fitted the moments in the interval $1 > \delta y > 0.1$. The slopes obtained for this reduced sample are given in Table 2c. They show the same behaviour as the ones in the full sample. Comparing our results with the slopes found in p-Emulsion interactions at 200 and 800 GeV/c [20], reproduced in Table 2d, we find that our slopes are considerably smaller. They are also considerably smaller than the slopes in M^+p interactions from the same experimental set-up (see Table 2e).

We are thus led to the conclusion that intermittency effects, as observed in the higher moments, are weak in positive meson induced interactions on Al and Au nuclei.

A relationship exists between the factorial moments of order i, and the parametrization of the multiplicity distribution (MD) in terms of a negative binomial distribution (NBD). If the MD is described by the NBD with parameters $\overline{n}$, the average multiplicity, and $1/k$, a measure of the width of the distribution, then the factorial moments can be expressed in the form

$$F_i = (1 + \frac{1}{k})(1 + \frac{2}{k}) \ldots (1 + \frac{(i-1)}{k}) \quad , \tag{7}$$

which implies that the higher order moments F_3, F_4,... can be expressed in terms of the moment F_2, with $\frac{1}{k} = F_2 - 1$. In ref. [14] we have shown that the MD's of M^+Al and M^+Au interactions are rather well represented by the NBD in restricted phase space intervals, separately in the forward and backward hemispheres. Fig. 4 shows

the factorial moments for the full sample with $-2 < y < 1$ (same data as in Fig. 2), with F_3 and F_4 calculated from F_2 according to (7). The shape of the calculated F_3 and F_4 indeed follows closely the shape of the experimental data, but the calculated values rise above the experimental ones for small δy, particularly for F_4. This can be caused by the truncation effect due to the limited statistics.

The limiting values of $< F_2 >$ for the experimental data are 1.43 (1.43) for M^+Al horizontal (vertical) averaging, and 1.47 (1.43) for M^+Au collisions, horizontal (vertical) averaging, leading to values of $\frac{1}{k} = F_2 - 1$ which are fully compatible with the experimentally observed ones of 0.43 for M^+Al and 0.46 for M^+Au interactions; however, we noticed that these NBD-fits are not of good quality.

4 Two-particle rapidity correlations

The two-particle correlation function in rapidity space has been extensively studied in hadron-hadron interactions (see e.g. [21a] for a review and for references to the original papers and [21b] for recent data). Much less attention has been paid to these correlations in hadron-nucleus interactions and no data exist for incident π^+ or K^+ mesons above 10 GeV/c. The review article of Fredriksson et al. [22] lists the publications with data from π^- and p beams.

The correlation function is defined as

$$R(y_1, y_2) = \frac{N_{ev}(d^2N)/(dy_1 dy_2)}{(dN/dy_1)(dN/dy_2)} - 1 \quad . \tag{8}$$

In particular we will examine the function $R(y, 0)$ at $y_2 = 0$ for all charge combinations, i.e. charged-charged, positive-positive, negative-negative and positive-negative.

Figure 5 (6) shows the correlation functions $R(y, 0)$ for M^+Al (M^+Au) interactions for all four charge combinations for the full data samples. The dash-dotted lines are derived from the FRITIOF model [18]. The following observations can be made.

- In contrast to hadron-hadron interactions, the correlation function is not symmetric w.r.t. $y = 0$, but is larger in the backward c.m. hemisphere, where intranuclear cascading contributes significantly to particle production.
- For each of the charge combinations, the correlation function is the same within errors for interactions on Al and on Au.
- The value $R(y_1 = 0, y_2 = 0)$, tabulated in Table 3, is of the same magnitude in meson-nucleus interactions as in $h - p$ interactions at comparable energies [23,24].

- The FRITIOF model reproduces rather well the correlations for M^+Au interactions, with a minor underestimation around $y = 0$. The shape of the correlation functions is also quite well described for M^+Al interactions, but the predicted values tend to be too large. In contrast to the data, the correlation values at fixed y decrease in the model with increasing atomic mass of the target nucleus.

It is well known (see [25] for a review and refs. to the original papers) that the inclusive two-particle correlations can be large and positive, even if no correlation exists in the semi-inclusive data samples. Studying the variation of the correlation $R(y,0)$ as a function of n_s, the multiplicity of shower particles, i.e. identified protons and electrons are excluded, we find that the large values of $R(y,0)$ are due to the mixing of different multiplicities. In Fig. 7 we show $R_{CC}(y,0)$ in 4 intervals of charge multiplicity: a) $n_s \leq 8$, b) $9 \leq n_s \leq 12$, c) $13 \leq n_s \leq 17$ and d) $n_s \geq 18$ for M^+Al collisions. The charge-charge correlations are large and positive for the smallest multiplicities only (Fig. 7a), and either small or negative for average or large multiplicities (Fig. 7b-d). The same observation can be made for M^+Au interactions (Fig. 8), where the correlations are systematically slightly larger than in M^+Al (compare Fig. 8a with 7a, 8b with 7b, etc). Comparing the FRITIOF predictions (dash-dotted lines on Figs. 7 and 8) with the data, we notice that now the predictions are systematically low at small y, both for the Au and the Al data, in contrast to the full sample of M^+Au (Fig. 6). We are thus led to the conclusion that the rather good agreement of FRITIOF with the inclusive data is a coincidence.

Recently, De Wolf [11] has pointed to the relationship between the normalized factorial moment of order 2, and the two-body rapidity correlation for small δy:

$$F_2 = 1 + R(0,0). \tag{9}$$

The experimental values of $R(0,0)$ are given in Table 3. Combining (7) for $i = 2$ and (9), we expect $1/k = R(0,0)$. The averages of the values of $1/k$, derived from F_2 in the limit of small intervals of rapidity, are indeed compatible with the observed $R_{CC}(0,0)$ values.

5 Bose–Einstein correlations

The study of Bose–Einstein correlations has a long history, but relatively few definite and unambiguous conclusions could be drawn[2]. Recent reviews are given in ref. [27]. In [28], results were published on Bose–Einstein correlations in K^+p and π^+p

[2]Already in 1968, Hagedorn and Ranft [26] stated that "The real significance and influence of the Bose–Einstein effect is still not understood". This statement is still valid, 22 years later. Hagedorn and Ranft added a quotation from R. Becker: "Gott schütze uns vor dem Mann, der eines Tages die vollständige Lösung präsentiert"

interactions at 250 GeV/c, derived from the same experiment with the same set-up as the present one, using two different parametrizations of the data. In the same paper the results are compared to earlier results at other energies and for other types of collisions.

One considers the ratio of the distribution of a suitable variable for like-sign pions, to this distribution for a reference sample. The choice of the variable determines the form of the parametrization:

1. the Kopylov-Podgoretskii parametrization [29]:

$$R(q_T) = \gamma \left[1 + 4\lambda J_1^2(\beta q_T)/(\beta q_T)^2\right](1 + \delta q_T) \tag{10}$$

at small values of $q_0 = |E_1 - E_2|$, the energy difference of the two pions considered. The variable q_T is the length of the component of the three-vector $\vec{q} = \vec{p_1} - \vec{p_2}$, transverse to $\vec{p_1} + \vec{p_2}$; J_1 is the first order Bessel function. The fit parameters are the normalization γ, the correlation strength λ, the spatial dimension in the c.m.s. of the pion source β (with $r = 0.197\beta$ fm) and δ, introduced to account for the slow variation of the background.

2. the Goldhaber parametrization [30]

$$R(Q^2) = \gamma \left[1 + \lambda \exp(-\beta Q^2)\right](1 + \delta Q^2) \tag{11}$$

with $Q^2 = -(p_1 - p_2)^2 = M^2 - 4m_\pi^2$ where M is the invariant mass of the pion pair and the fit parameters have the same meaning as in (10), except for the radius r which is given by $r = 0.197\sqrt{\beta}$fm and refers to the reference frame where the pion pair is at rest.

The reference sample should be constructed in such a way that it has the same characteristics as the like pion sample, except for the Bose–Einstein correlations. Several possibilities exist. The two mostly used are the "unlike" sample and the "mixed" sample. The "unlike" sample is composed of all combinations of unlike-charge within the same event and the "mixed" sample is constructed by combining pions from one event with pions of the same charge, randomly chosen in other events with approximately the same charge multiplicity.

Since protons are identified only up to a momentum $p_{\rm lab}$=1.2 GeV/c, we expect some contamination of protons in the sample of positive pions, and thus also in the reference sample. Moreover, an appreciable number of photons, decay products of neutral pions, will convert into e^-e^+ pairs, due to the finite thickness of the nuclear targets. With the identification of electrons and positrons limited to $p_{\rm lab} \approx$ 200 MeV/c, the average number of undetected electrons or positrons in the sample was estimated to be 1.05 (0.16) per event in the Au (Al) sample. They contribute particularly to the region of small Q^2 and q_T values, i.e. precisely in the region where

the Bose–Einstein effect is expected to show up, and the unlike reference sample is therefore not suitable for study of Bose–Einstein correlations in nuclear targets.

Fig. 9 shows the ratio $R(q_T)$, obtained with the mixed reference sample, for positive and negative like-pion combinations and both targets. In all plots of Fig. 9, a significant enhancement is observed at small q_T values. Fits according to formula (10) and for $q_0 \leq 0.2$ GeV/c are superimposed. No stable fit could be obtained for negative pairs in the Au-sample (Fig. 9c). The fit parameters are collected in Table 4. The value of the radius r of the pion emission volume is considerably larger for negative than for positive pion combinations. This may be due to the contamination of the positive pion sample by unidentified fast protons, which reduce the signal (the "coherence" factor λ is considerably smaller). Considering also M^+p interactions [28], from the same experiment and treated in the same way, we observe a strong increase of the radius r with increasing atomic mass number A.

The above observation is in contradiction with results published by de Marzo et al. [31], who found no A dependence for both incident proton and $\overline{p}$ on proton and Xe targets. The authors of ref. [31] however used a reference sample constructed by randomly mixing the transverse momentum components of pions in each event and then recalculating the q_T variable in the c.m. system. The contaminations of the positive pion sample mentioned above, i.e. unidentified protons with momentum above $p_{\rm lab} = 600$ MeV/c (their limit of identification), and positrons (and electrons) from converted gammas, tend to decrease the Bose–Einstein effect and may in part explain the discrepancies. Moreover, in the Appendix of ref. [28], we have shown by Monte Carlo generation that the method of reshuffling p_T components leaves a "Bose–Einstein–like" correlation in the reference sample, because the longitudinal momentum components remain the same.

With the selection criteria used, the event passing rate decreases approximately linearly with charged multiplicity and the accepted loss of tracks (20%) may lead to a considerable number of tracks lost for high multiplicity events. We therefore show in Fig. 10 the ratios $R(q_t)$ for events with total charge multiplicity $6 \leq n_{ch} < 20$ where the number of not well reconstructed tracks is at most three. Table 4 also gives the results of fitting (10) to this sample. The radii r are compatible within error for positive and for negative pion pairs; they still increase with A.

The Goldhaber parametrization (11) in terms of the variable Q^2, seems not adequate for $h - A$ interactions, as appears from Fig. 11 where we plot eq. (11) for $\lambda = 0.3$, $\delta = 0.$ and r ranging from 0.5fm to 2.5fm. Extremely precise data are required to be able to distinguish between radii larger than about 1 fm.

A different approach to Bose–Einstein correlations is advocated by Weiner [32], based on quantum statistical considerations and assuming the particle fields to be a superposition of a chaotic and a coherent part. A chaoticity parameter p is introduced, being $p = < n_{\rm chaotic} > / < n_{\rm total} >$, and assuming a gaussian form for the

fields, he derives the correlation function

$$C_2(\Delta y) = 1 + 2p(1-p)\exp[-(\Delta y)^2 r^2] + p^2 \exp[-2(\Delta y)^2 r^2] \qquad (12)$$

where y is a "stationary" but not uniquely determined variable and r the conjugate "correlation length". This parametrization was used in [33] to fit data on pp and $p\overline{p}$ interactions at $\sqrt{s}$ =53 and 63 GeV, using the rapidity difference and Q as variables.

Fig. 12 shows the two-body correlation for M^+Al and M^+Au collisions as a function of $y_{\rm diff} = |y_1 - y_2|$ for negative pion pairs with a mixed reference sample. The rapidity variable can be considered as a stationary variable in the interval $-1.8 < y < 1$ where the density of negative pions varies by less than 30% [15]. These distributions are fitted with the form

$$R(y_{\rm diff}) = \gamma\left(1 + 2p(1-p)\exp[-(y_{\rm diff})^2 r^2] + p^2 \exp[-2(y_{\rm diff})^2 r^2]\right) \qquad (13)$$

The results of the fits are collected in Table 5. The correlation length r is about one in meson–nucleus interactions, to be compared to 1.6 in pp and $p\overline{p}$ interactions [33]. The chaoticity parameter p is only 0.06, implying that (13) is in practice reduced to a single gaussian term. This would imply that particle production happens almost exclusively in a coherent way.

6 Summary

Results are presented, based on 4200 π^+/K^+ interactions on Al and 3700 on Au at an incident momentum of 250 GeV/c, measured with the european hybrid spectrometer. The main results are the following.

- The normalized factorial moments (eq. 4) F_2 and F_3 rise very slowly with decreasing interval δy and F_4 is constant or slowly decreasing. If intermittency is present at all, it is a very weak effect, particularly in the higher moments.

- The two-particle rapidity correlation function $R(y, 0)$ is the same for Al and Au, but different from that for elementary collisions: it is larger in the backward c.m. hemisphere. The FRITIOF model reproduces rather well the inclusive correlation functions but not the semi-inclusive ones.

- Bose–Einstein correlations are observed, leading to radii of the pion emission volume of 2.3 fm (4.8 fm) in Al (Au) for events with charge multiplicity less than 20, with the Kopylov–Podgoretskii parametrization (10). If the two-particle correlations are interpreted in terms of Weiner's quantum statistical model, we arrive at a chaoticity parameter of 0.06 and a correlation length of about one, much smaller than in pp collisions at $\sqrt{s}$=53 and 63 GeV.

Aknowledgments

We are indebted to the CERN SPS, beam and EHS crews for their support during the run of the experiment. It is a pleasure to thank the scanning and measuring staffs of our laboratories. The contributions of the groups at Aachen, Helsinki and Warsaw to the earlier phase of this experiment is gratefully acknowledged.

7 References

1. A. Białas, R. Peschanski: Nucl. Phys. **B273** (1986) 703
2. A. Białas, R. Peschanski: Nucl. Phys. **B308** (1988) 857
3. A. Białas, R. Peschanski: Phys. Lett. **B207** (1988) 59
4. a) W. Kittel, R Peschanski: Nucl. Phys. Proc. Suppl. **16** (1990) 445
   b) B. Buschbeck, P. Lipa: Mod. Phys. Lett. **A4** (1989) 1871
5. I. Derado et al.: Z. Phys. C – Particles and Fields, **C47** (1990) 23
6. W. Ochs, J. Wosiek: Phys. Lett. **B224** (1988) 617
   B. Andersson, P. Dahlqvist, G. Gustafson: Phys. Lett. **B214** (1988) 604
7. a) J. Dias de Deus: preprint CERN-TH 5317 (1989)
   b) P. Carruthers, I. Sarcevic: Phys. Rev. Lett. **63** (1989) 1562
8. L. Van Hove: Phys. Lett. **B232** (1989) 509
9. A. Capella, K. Fialkowski, A. Krzywicki: Phys. Lett. **B230** (1989) 149
10. M. Gyulassy in *"Multiparticle Dynamics, Festschrift for Léon Van Hove,* Eds. A. Giovannini, W. Kittel, World Scientific, Singapore, 1990, p. 479
11. E.A. De Wolf: *Intermittency, negative binomials and two-particle correlations*, Brussels Universities preprint IIHE-ULB-VUB-90/01, to appear in Acta Phys. Pol. B
12. a) M. Adamus et al. (NA22): Z. Phys. C – Particles and Fields, **C32** (1986) 475
    b) P. van Hal: *Particle production in hadron-proton interactions at 250 GeV/c incident beam momentum*, Ph.D. thesis, Nijmegen 1987 (unpublished)
13. I.V. Ajinenko et al. (NA22): Z. Phys. C – Particles and Fields, **42** (1989) 377
14. I.V. Ajinenko et al. (NA22): Z. Phys. C – Particles and Fields, **46** (1990) 569
15. N.M. Agababyan et al. (NA22): *Rapidity and transverse momentum structure in π^+ and K^+ collisions with Al and Au nuclei at 250 GeV/c*, to be submitted to Z. Phys. C
16. I.V. Ajinenko et al. (NA22): Phys. Lett. **B222** (1989) 306
17. K. Fiałkowski, B. Wosiek and J. Wosiek, Acta Phys. Pol. **B20** (1989) 639

18. B. Andersson, G. Gustafson, B. Nilsson-Almqvist: Lund preprint LU TP 86-3

19. a) B. Buschbeck, P. Lipa: *Intermittency studies in $\bar{p}p$ collisions at $\sqrt{s}$ = 630 GeV/c and a comparison with heavy ion reactions*, HEPHY-PUB 535/90 preprint, Vienna.

    b) A. Białas: *Intermittency '90,* Invited Talk at "Quark Matter '90", Menton, 7-11 May, to be published in Nucl. Phys. A (Proc. Suppl.)

20. R. Hołynski et al. (KLM): Phys. Rev. Lett. **62** (1989) 733

21. a) J. Giacomelli: Phys. Reports **55** (1979) 1

    b) R.E. Ansorge et al. (UA5): Z. Phys. C – Particles and Fields, **37** (1988) 191

22. S. Fredriksson et al.: Phys. Reports **144** (1987) 187

23. I.V. Ajinenko et al. (NA22): "*Rapidity correlations in K^+p and π^+p interactions at 250 GeV/c*", submitted to Z. Phys. C

24. J.L. Bailly et al. (NA23): Z. Phys. C – Particles and Fields, **C40** (1988) 13

25. J. Whitmore, Phys. Reports **27** (1976) 187

26. R. Hagedorn, J. Ranft: Supp. Nuovo Cim. **6** (1968) 169

27. "*Hadronic Matter in Collision*", Eds. P. Carruthers, D. Strottman, World Scientific, Singapore, 1986; see contributions of G. Goldhaber, p. 3 and W.A. Zajc, p. 43

28. M. Adamus et al. (NA22): Z. Phys. C – Part. and Fields, **37** (1988) 347

29. G.I. Kopylov, M.I. Podgoretskii: Sov. J. Nucl. Phys. **15** (1972) 219; **18** (1974) 336; G.I. Kopylov: Phys. Lett. **B50** (1974) 472

30. G. Goldhaber et al.: Phys. Rev. Lett. **3** (1959) 181; Phys. Rev. **120** (1960) 300

31. C. de Marzo et al. (NA5): Phys. Rev. **D29** (1984) 363

32. R.M. Weiner: Phys. Lett. **B232** (1989) 278 and references therein

33. K. Kulka, B. Lörstad: Z. Phys. C – Particles and Fields **45** (1990) 581

Table 1. The experimental factorial moments F_i in the interval $-2 < y < 1$, for the full M^+Al sample (horizontal averaging **a**) and vertical averaging **c**)) and the full M^+Au sample (horizontal averaging **b**) and vertical averaging **d**)).

a) Full M^+Al sample, horizontal averaging

δy	F_2	F_3	F_4
3.000	1.29 ± 0.03	2.04 ± 0.08	3.80 ± 0.25
1.500	1.35 ± 0.03	2.29 ± 0.09	4.61 ± 0.36
1.000	1.38 ± 0.01	2.39 ± 0.02	4.88 ± 0.00
0.750	1.39 ± 0.01	2.47 ± 0.06	5.43 ± 0.35
0.600	1.40 ± 0.01	2.55 ± 0.06	5.71 ± 0.29
0.500	1.40 ± 0.01	2.49 ± 0.06	5.37 ± 0.29
0.429	1.40 ± 0.01	2.54 ± 0.07	5.55 ± 0.39
0.375	1.41 ± 0.01	2.55 ± 0.07	5.59 ± 0.41
0.333	1.41 ± 0.01	2.57 ± 0.08	5.68 ± 0.61
0.300	1.41 ± 0.01	2.52 ± 0.08	5.35 ± 0.40
0.273	1.41 ± 0.01	2.47 ± 0.09	5.28 ± 0.58
0.250	1.40 ± 0.01	2.46 ± 0.08	5.10 ± 0.42
0.231	1.42 ± 0.02	2.60 ± 0.10	5.90 ± 0.66
0.214	1.42 ± 0.02	2.57 ± 0.09	5.38 ± 0.45
0.200	1.42 ± 0.02	2.57 ± 0.10	5.75 ± 0.58
0.188	1.42 ± 0.02	2.54 ± 0.10	5.30 ± 0.57
0.176	1.44 ± 0.02	2.68 ± 0.11	5.62 ± 0.52
0.167	1.42 ± 0.02	2.55 ± 0.13	5.84 ± 1.10
0.158	1.43 ± 0.02	2.60 ± 0.12	5.64 ± 0.68
0.150	1.42 ± 0.02	2.53 ± 0.11	5.25 ± 0.61
0.143	1.43 ± 0.02	2.62 ± 0.14	6.02 ± 0.98
0.136	1.42 ± 0.02	2.53 ± 0.12	5.09 ± 0.66
0.130	1.43 ± 0.02	2.63 ± 0.14	5.72 ± 0.89
0.125	1.43 ± 0.02	2.58 ± 0.14	5.56 ± 1.04
0.120	1.43 ± 0.02	2.67 ± 0.14	5.94 ± 0.97
0.115	1.42 ± 0.02	2.56 ± 0.14	5.32 ± 0.76
0.111	1.43 ± 0.02	2.55 ± 0.14	5.12 ± 0.75
0.107	1.43 ± 0.02	2.64 ± 0.15	5.72 ± 0.85
0.103	1.44 ± 0.02	2.57 ± 0.15	5.18 ± 0.82
0.100	1.43 ± 0.02	2.60 ± 0.16	5.65 ± 1.24

b) Full M^+Au sample, horizontal averaging

δy	F_2	F_3	F_4
3.000	1.33 ± 0.03	2.15 ± 0.08	3.99 ± 0.22
1.500	1.42 ± 0.03	2.63 ± 0.11	6.04 ± 0.43
1.000	1.44 ± 0.00	2.69 ± 0.02	6.20 ± 0.18
0.750	1.44 ± 0.01	2.75 ± 0.06	6.66 ± 0.41
0.600	1.45 ± 0.01	2.75 ± 0.05	6.50 ± 0.41
0.500	1.46 ± 0.01	2.79 ± 0.05	6.60 ± 0.36
0.429	1.46 ± 0.01	2.81 ± 0.06	6.77 ± 0.40
0.375	1.46 ± 0.01	2.81 ± 0.07	6.73 ± 0.40
0.333	1.46 ± 0.01	2.86 ± 0.07	6.88 ± 0.41
0.300	1.46 ± 0.01	2.83 ± 0.08	6.87 ± 0.56
0.273	1.47 ± 0.01	2.84 ± 0.08	6.82 ± 0.49
0.250	1.45 ± 0.01	2.75 ± 0.07	6.20 ± 0.31
0.231	1.45 ± 0.01	2.72 ± 0.05	5.81 ± 0.22
0.214	1.46 ± 0.01	2.78 ± 0.07	6.28 ± 0.32
0.200	1.46 ± 0.01	2.80 ± 0.08	6.36 ± 0.51
0.188	1.47 ± 0.01	2.90 ± 0.09	6.73 ± 0.42
0.176	1.47 ± 0.01	2.87 ± 0.08	6.33 ± 0.33
0.167	1.47 ± 0.02	2.85 ± 0.09	6.48 ± 0.42
0.158	1.47 ± 0.01	2.83 ± 0.09	6.55 ± 0.47
0.150	1.48 ± 0.02	2.87 ± 0.10	6.49 ± 0.52
0.143	1.47 ± 0.02	2.75 ± 0.10	5.94 ± 0.63
0.136	1.47 ± 0.02	2.89 ± 0.12	7.17 ± 0.86
0.130	1.48 ± 0.02	2.95 ± 0.13	7.04 ± 0.86
0.125	1.47 ± 0.02	2.84 ± 0.11	6.43 ± 0.67
0.120	1.45 ± 0.02	2.72 ± 0.10	5.80 ± 0.51
0.115	1.47 ± 0.02	2.80 ± 0.10	5.65 ± 0.50
0.111	1.48 ± 0.02	2.89 ± 0.12	6.57 ± 0.74
0.107	1.48 ± 0.02	3.00 ± 0.14	7.43 ± 0.89
0.103	1.47 ± 0.02	2.74 ± 0.12	5.84 ± 0.65
0.100	1.47 ± 0.02	2.83 ± 0.14	7.04 ± 1.12

c) Full M^+Al sample, vertical averaging

δy	F_2	F_3	F_4
3.000	1.29 ±0.03	2.04 ±0.08	3.80 ±0.25
1.500	1.35 ±0.03	2.32 ±0.09	4.77 ±0.37
1.000	1.38 ±0.02	2.40 ±0.08	4.91 ±0.31
0.750	1.39 ±0.02	2.45 ±0.09	5.30 ±0.42
0.600	1.40 ±0.02	2.53 ±0.09	5.55 ±0.39
0.500	1.39 ±0.02	2.47 ±0.09	5.30 ±0.40
0.429	1.40 ±0.02	2.50 ±0.09	5.31 ±0.43
0.375	1.40 ±0.02	2.51 ±0.10	5.31 ±0.43
0.333	1.41 ±0.02	2.51 ±0.10	5.25 ±0.56
0.300	1.40 ±0.02	2.46 ±0.10	4.99 ±0.44
0.273	1.40 ±0.02	2.41 ±0.10	4.85 ±0.53
0.250	1.40 ±0.02	2.42 ±0.10	4.78 ±0.47
0.231	1.41 ±0.02	2.53 ±0.11	5.35 ±0.62
0.214	1.42 ±0.02	2.50 ±0.11	4.91 ±0.50
0.200	1.41 ±0.02	2.52 ±0.12	5.38 ±0.64
0.188	1.41 ±0.02	2.51 ±0.11	4.91 ±0.54
0.176	1.43 ±0.03	2.60 ±0.12	5.12 ±0.53
0.167	1.41 ±0.03	2.49 ±0.13	5.25 ±0.86
0.158	1.42 ±0.03	2.50 ±0.12	5.01 ±0.63
0.150	1.42 ±0.03	2.46 ±0.12	4.70 ±0.58
0.143	1.42 ±0.03	2.55 ±0.14	5.40 ±0.81
0.136	1.41 ±0.03	2.50 ±0.13	4.77 ±0.67
0.130	1.42 ±0.03	2.57 ±0.14	5.15 ±0.82
0.125	1.42 ±0.03	2.53 ±0.14	5.02 ±0.96
0.120	1.42 ±0.03	2.58 ±0.15	5.31 ±0.93
0.115	1.42 ±0.03	2.47 ±0.14	4.71 ±0.66
0.111	1.42 ±0.03	2.47 ±0.14	4.61 ±0.68
0.107	1.42 ±0.03	2.56 ±0.15	4.96 ±0.75
0.103	1.43 ±0.03	2.50 ±0.15	4.65 ±0.77
0.100	1.43 ±0.03	2.54 ±0.16	5.05 ±1.11

d) Full M^+Au sample, vertical averaging

δy	F_2	F_3	F_4
3.000	1.33 ± 0.03	2.15 ± 0.08	3.99 ± 0.22
1.500	1.39 ± 0.03	2.47 ± 0.09	5.26 ± 0.34
1.000	1.40 ± 0.03	2.49 ± 0.09	5.29 ± 0.34
0.750	1.41 ± 0.02	2.53 ± 0.09	5.58 ± 0.44
0.600	1.41 ± 0.02	2.52 ± 0.09	5.42 ± 0.43
0.500	1.42 ± 0.02	2.57 ± 0.09	5.57 ± 0.40
0.429	1.42 ± 0.02	2.57 ± 0.09	5.66 ± 0.41
0.375	1.42 ± 0.02	2.58 ± 0.09	5.67 ± 0.42
0.333	1.43 ± 0.02	2.63 ± 0.09	5.78 ± 0.41
0.300	1.42 ± 0.02	2.60 ± 0.10	5.76 ± 0.50
0.273	1.43 ± 0.02	2.60 ± 0.09	5.69 ± 0.47
0.250	1.42 ± 0.02	2.53 ± 0.09	5.20 ± 0.36
0.231	1.42 ± 0.02	2.50 ± 0.09	4.89 ± 0.33
0.214	1.42 ± 0.02	2.55 ± 0.09	5.27 ± 0.38
0.200	1.42 ± 0.02	2.54 ± 0.09	5.21 ± 0.44
0.188	1.43 ± 0.02	2.67 ± 0.10	5.71 ± 0.44
0.176	1.44 ± 0.02	2.65 ± 0.10	5.45 ± 0.41
0.167	1.43 ± 0.02	2.59 ± 0.10	5.27 ± 0.43
0.158	1.43 ± 0.02	2.57 ± 0.10	5.38 ± 0.46
0.150	1.44 ± 0.02	2.65 ± 0.11	5.53 ± 0.48
0.143	1.44 ± 0.02	2.54 ± 0.11	5.08 ± 0.52
0.136	1.44 ± 0.02	2.69 ± 0.12	6.17 ± 0.68
0.130	1.45 ± 0.02	2.76 ± 0.13	6.25 ± 0.73
0.125	1.43 ± 0.02	2.62 ± 0.12	5.60 ± 0.64
0.120	1.42 ± 0.02	2.55 ± 0.12	5.33 ± 0.61
0.115	1.43 ± 0.02	2.60 ± 0.12	5.06 ± 0.64
0.111	1.44 ± 0.03	2.67 ± 0.13	5.70 ± 0.72
0.107	1.44 ± 0.03	2.76 ± 0.14	6.50 ± 0.85
0.103	1.43 ± 0.02	2.50 ± 0.12	4.94 ± 0.68
0.100	1.43 ± 0.03	2.56 ± 0.13	5.67 ± 0.84

Table 2. Fitted slopes f_i (eq. 6) of the fits for the experimental factorial moments F_i and for FRITIOF Monte Carlo events, in the interval $-2 < y < 1$, with the fits performed in the range $0.4 \geq \delta y > 0.1$ for **a)** the full M^+Al and M^+Au samples, horizontal averaging, **b)** same as a), but vertical averaging, **c)** a restricted sample with $n_{ch} \geq 10$ and fit in the range $1. \geq \delta y > 0.1$, bf d) $p\ Em$ data at 200 and 800 GeV/c from ref. [20] and **e)** M^+p interactions (from ref. [16]), fitted in the interval $1 \geq \delta y > 0.1$.

a) Full sample, horizontal averaging

	M^+Al		M^+Au	
	Data	Fritiof	Data	Fritiof
f_2	0.0140±0.0010	0.0003±0.0004	0.0091±0.0008	0.0043±0.0003
f_3	0.0243±0.0052	0.0175±0.0025	0.0103±0.0052	0.0058±0.0060
f_4	-0.0013±0.0221	0.0410±0.0110	-0.0515±0.0133	0.0270±0.0112

b) Full sample, vertical averaging

	M^+Al		M^+Au	
	Data	Fritiof	Data	Fritiof
f_2	0.0127±0.0014	-0.0003±0.0007	0.0099±0.0013	0.0036±0.0005
f_3	0.0169±0.0058	0.0075±0.0026	0.0198±0.0051	0.0026±0.0089
f_4	-0.0454±0.0297	0.0083±0.0154	-0.0152±0.0186	-0.0137±0.0231

c) Restricted sample, horizontal averaging

	M^+Al		M^+Au	
	Data	Fritiof	Data	Fritiof
f_2	0.0168±0.0262	0.0052±0.0011	0.0116±0.0019	0.0065±0.0010
f_3	0.0422±0.0076	0.0214±0.0041	0.0263±0.0059	0.0142±0.0029
f_4	0.0821±0.0147	0.0489±0.0118	-0.0044±0.0176	0.0171±0.0080

d) $p\ Em$ data from ref. [20]

	200 GeV/c	800 GeV/c
f_2	0.027±0.002	0.023±0.002
f_3	0.063±0.011	0.062±0.006
f_4	0.129±0.030	0.094±0.017

e) M^+p interactions, horizontal averaging

	M^+p
f_2	0.0127±0.0008
f_3	0.0499±0.0022
f_4	0.1480±0.0070

Table 3. The value of the two-body correlation function $R(y_1, y_2)$ for $y_1 = y_2 = y = 0$ for the full samples of events.

	M^+Al		M^+Au	
	Data	Fritiof	Data	Fritiof
CC	0.41±0.04	0.50±0.03	0.43±0.03	0.37±0.02
++	0.28±0.05	0.35±0.04	0.32±0.05	0.27±0.03
−−	0.35±0.06	0.37±0.04	0.37±0.06	0.31±0.03
+−	0.49±0.06	0.65±0.04	0.52±0.06	0.44±0.03

Table 4. Fit results for the Kopylov-Podgoretskii parametrization (eq. 9) to the ratio $R(q_t)$ for like-pion distributions. The results for M^+p interactions are reproduced from ref. [28]

Sample	Charge	λ	β (GeV/c)$^{-1}$	r (fm)	γ	δ (GeV/c)$^{-1}$	χ^2/NDF
M^+p	−−	0.30 ± 0.03	7.0 ± 0.5	1.4 ± 0.1	0.91 ± 0.03	0.04 ± 0.05	42/36
M^+Al	−−	0.48 ± 0.10	17 ± 2	3.3 ± 0.4	1.01 ± 0.03	-0.11 ± 0.05	54/45
$n_{ch} \geq 6$	++	0.22 ± 0.06	8.4 ± 1.2	1.7 ± 0.2	0.95 ± 0.04	0.03 ± 0.06	37/45
M^+Au	−−	−	−	−	−	−	−
$n_{ch} \geq 6$	++	0.25 ± 0.06	16 ± 3	3.2 ± 0.5	1.02 ± 0.02	0.46 ± 0.17	37/45
M^+Al	−−	0.41 ± 0.11	12 ± 2	2.3 ± 0.3	0.99 ± 0.05	-0.11 ± 0.08	26/45
$6 \leq n_{ch} < 20$	++	0.19 ± 0.09	13 ± 4	2.5 ± 0.7	1.05 ± 0.04	-0.17 ± 0.05	42/45
M^+Au	−−	0.28 ± 0.17	24 ± 6	4.8 ± 1.1	1.07 ± 0.04	-0.22 ± 0.06	36/45
$6 \leq n_{ch} < 20$	++	0.37 ± 0.13	18 ± 4	3.5 ± 0.8	1.00 ± 0.22	-0.06 ± 0.14	26/45

Table 5. Fit results for the Weiner parametrization (13) to the ratio $R(y_{\rm diff})$.

Sample	Charge	p	r	γ	χ^2/NDF
M^+Al	−−	0.06 ± 0.02	0.92 ± 0.36	0.93 ± 0.03	41/22
M^+Au	−−	0.06 ± 0.01	0.97 ± 0.21	0.94 ± 0.02	26/22

8 Figure captions

Fig. 1 Average errors $< \Delta y >$ of the rapidity variable as a function of rapidity for a) negative particles in the Au sample, b) positives in Au. c) negatives in Al and d) positives in Al.

Fig. 2 Normalized horizontal averaged factorial moments of order 2 to 4 for a) M^+Al, b) M^+Au interactions and normalized vertical averaged factorial moments of order 2 to 4 for c) M^+Al, d) M^+Au interactions for the full samples. The full line corresponds to the fit of eq. (6). The dash-dotted line is the prediction of the FRITIOF model.

Fig. 3 Dependence of the slope f_2 on the rapidity density dn/dy.

Fig. 4 The same data as in Fig. 2 with F_3 and F_4 calculated from eq. (7).

Fig. 5 $R(y,0)$ for M^+Al interactions, with the following charge combinations: a) CC, b) ++, c) $--$ and d) $+-$. The dash-dotted lines are the predictions of the FRITIOF model.

Fig. 6 As in Fig. 5 for M^+Au interactions.

Fig. 7 $R(y,0)$ for CC combinations in four intervals of charge multiplicity a) $n_s \leq 8$, b) $9 \leq n_s \leq 12$. b) $13 \leq n_s \leq 17$ and d) $n_s \geq 18$ for M^+Al collisions The dash-dotted lines are the predictions of the FRITIOF model.

Fig. 8 As in Fig. 7 for M^+Au collisions

Fig. 9 The ratio $R(q_T)$ for like pions with a "mixed" reference sample a) $--$ in $M + Al$, b) ++ in M^+Al, c) $--$ in M^+Au and d) ++ in M^+Au.

Fig. 10 As in Fig. 8, for the sample with $6 \leq n_{ch} < 20$.

Fig. 11 $R(Q^2)$ according to eq. (11) with $\lambda = 0.3$, $\delta = 0$ and r varying from 0.5 to 2.5 fm.

Fig. 12 The ratio $R(y_{\mathrm{diff}})$ for negative like-pion combinations with a mixed reference sample for a) M^+Al, b) M^+Au interactions.

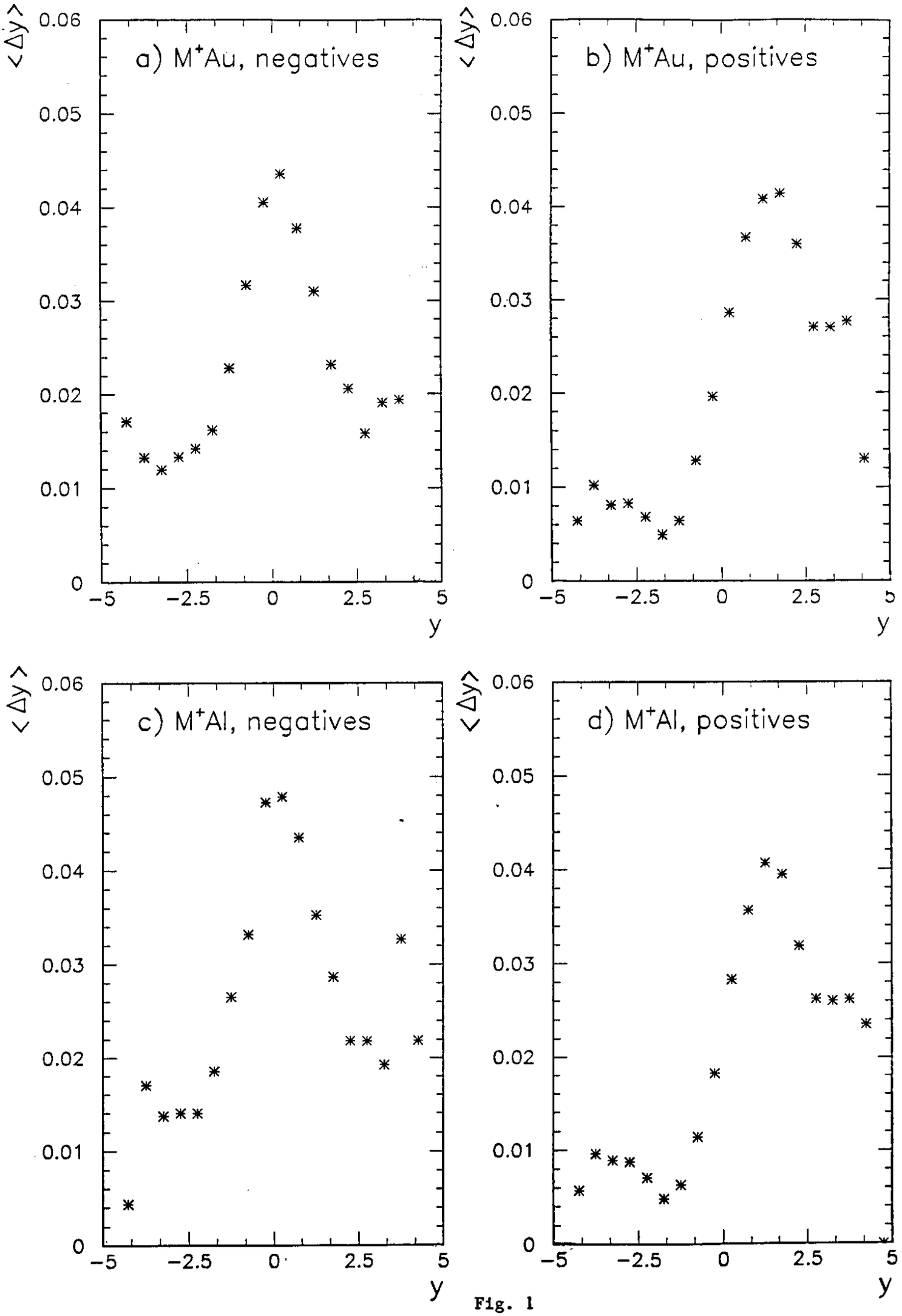
a) M+Au, negatives
b) M+Au, positives
c) M+Al, negatives
d) M+Al, positives
<Δy>
y
0.06
0.05
0.04
0.03
0.02
0.01
0
−5
−2.5
0
2.5
5

Fig. 1

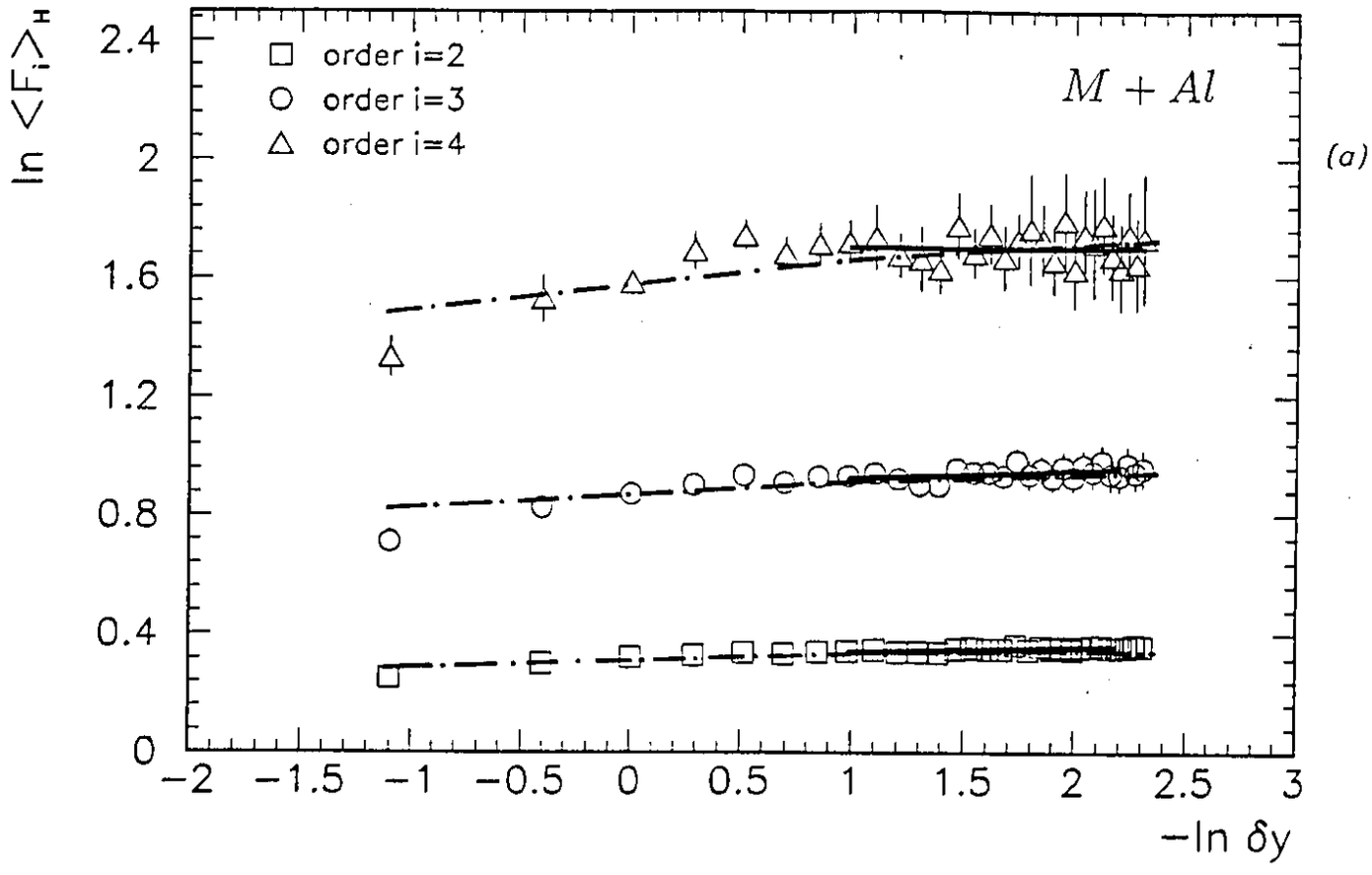
ln <F_i>^H
order i=2
order i=3
order i=4
M + Al
(a)
2.4
2
1.6
1.2
0.8
0.4
0
−2
−1.5
−1
−0.5
0
0.5
1
1.5
2
2.5
3
−ln δy

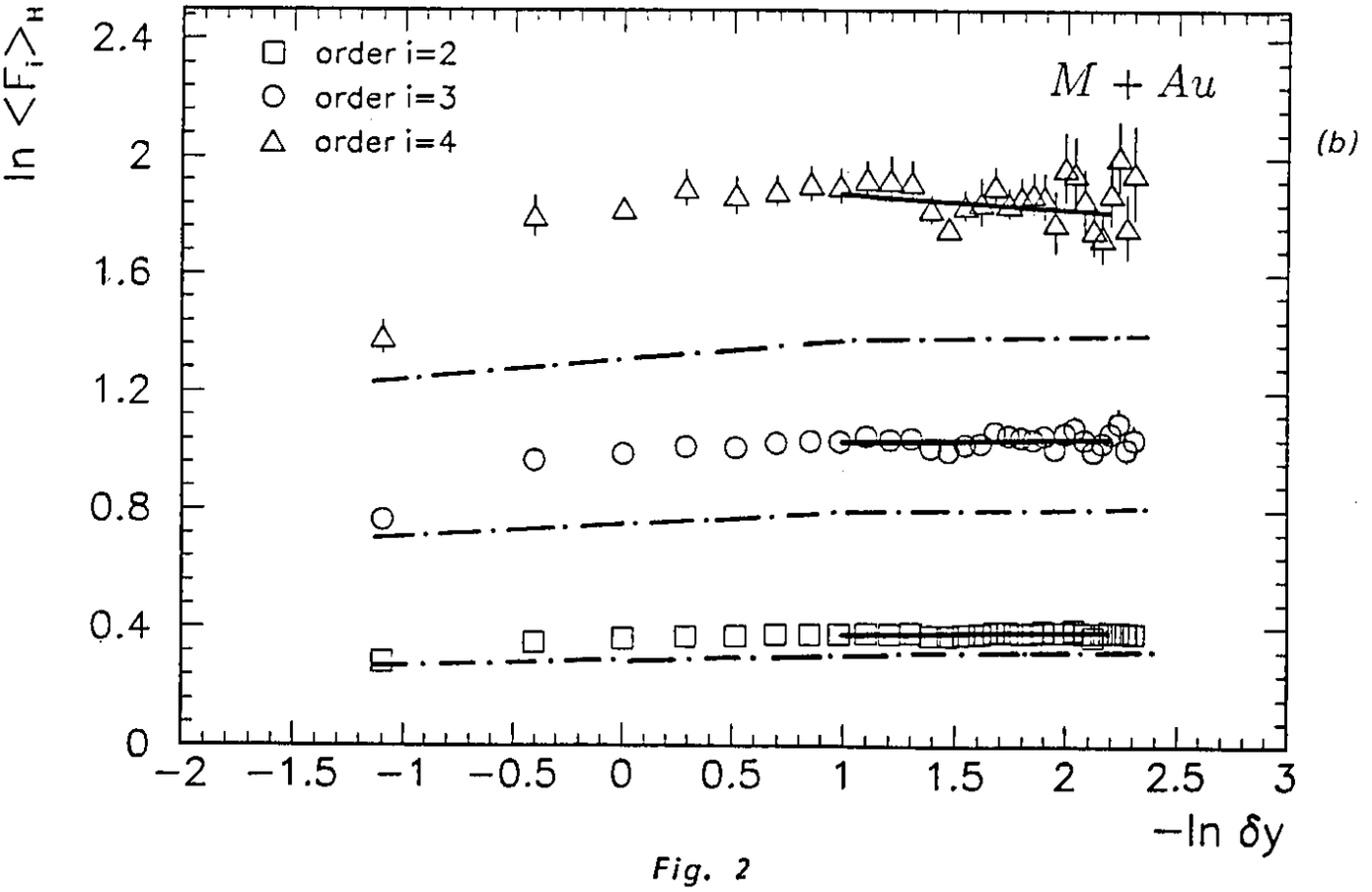
ln <F_i>^H
order i=2
order i=3
order i=4
M + Au
(b)
2.4
2
1.6
1.2
0.8
0.4
0
−2
−1.5
−1
−0.5
0
0.5
1
1.5
2
2.5
3
−ln δy

Fig. 2

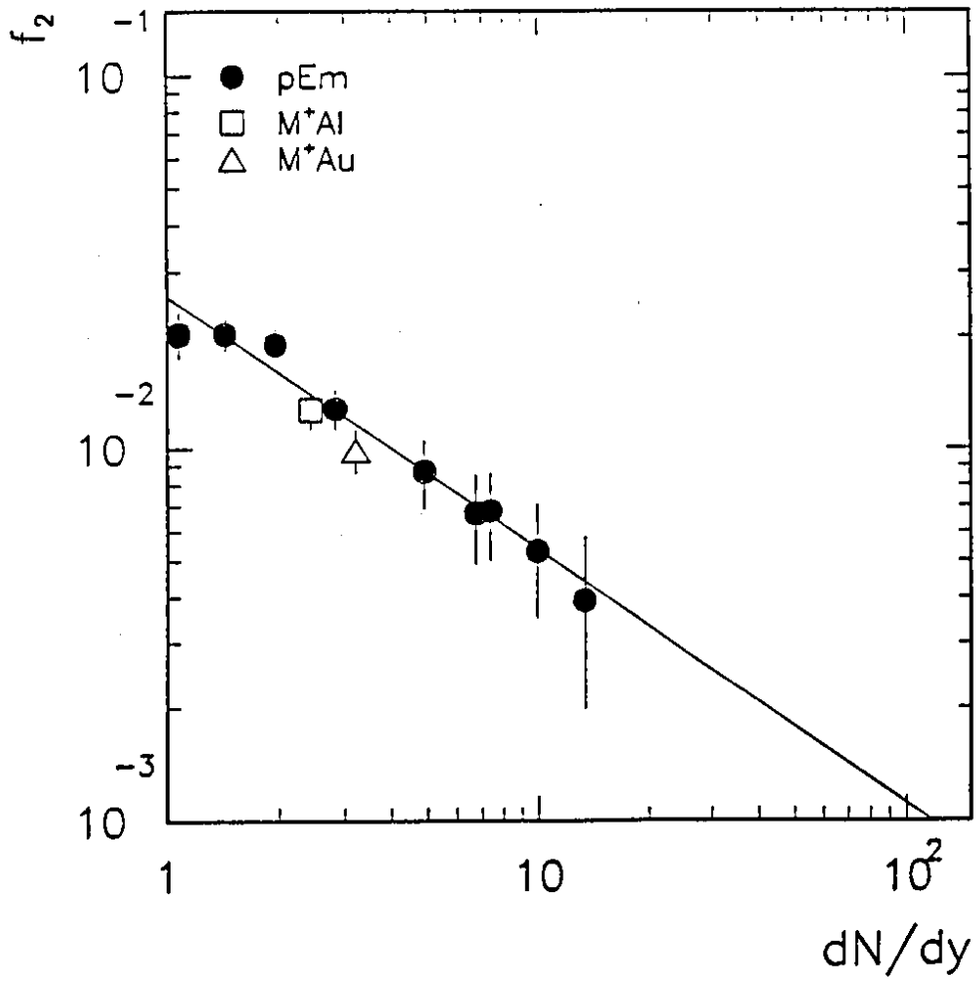

Fig. 3

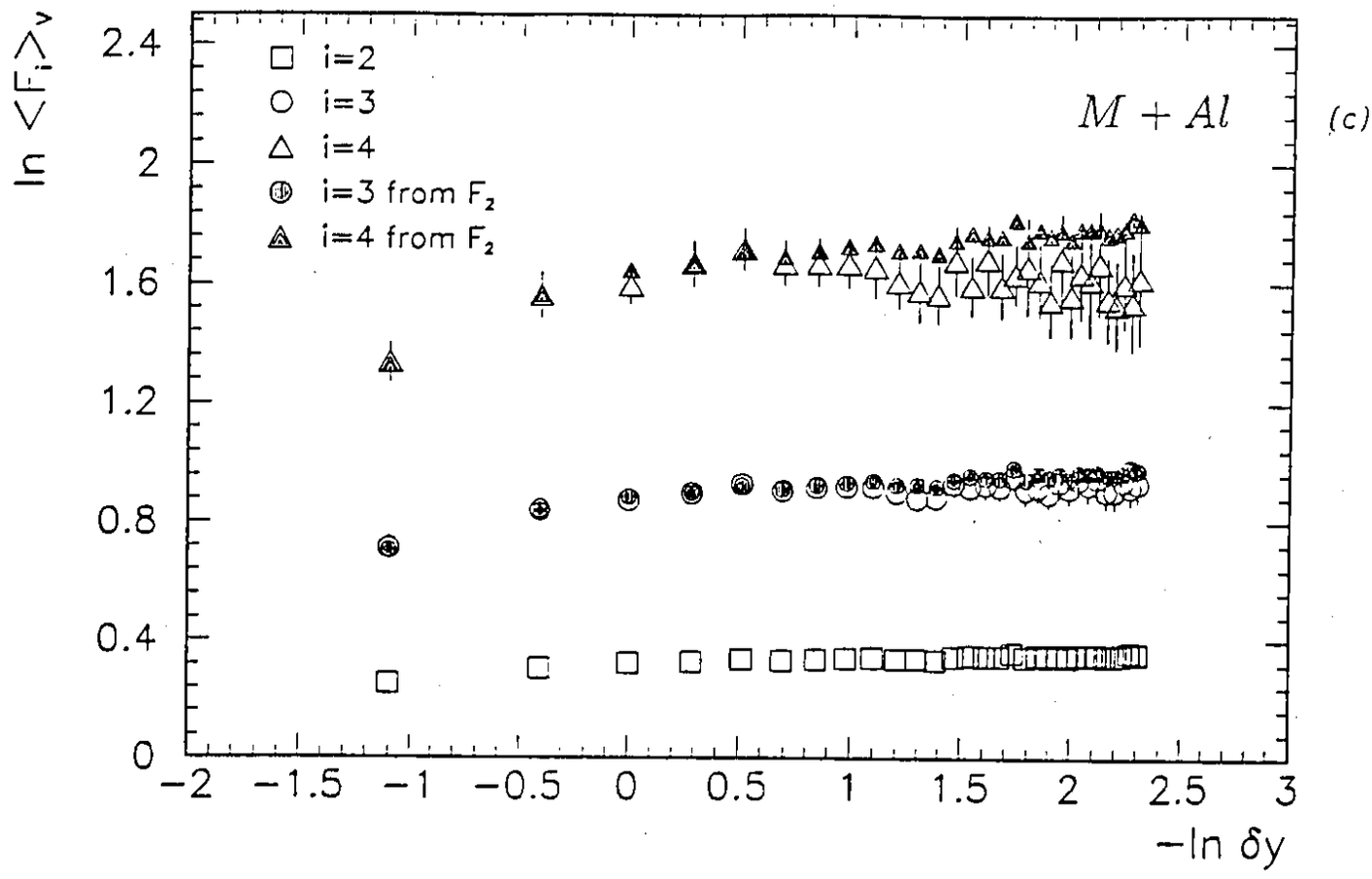
ln <F_i>_v
2.4
2
1.6
1.2
0.8
0.4
0
i=2
i=3
i=4
i=3 from F_2
i=4 from F_2
M + Al
(c)
−2
−1.5
−1
−0.5
0
0.5
1
1.5
2
2.5
3
−ln δy

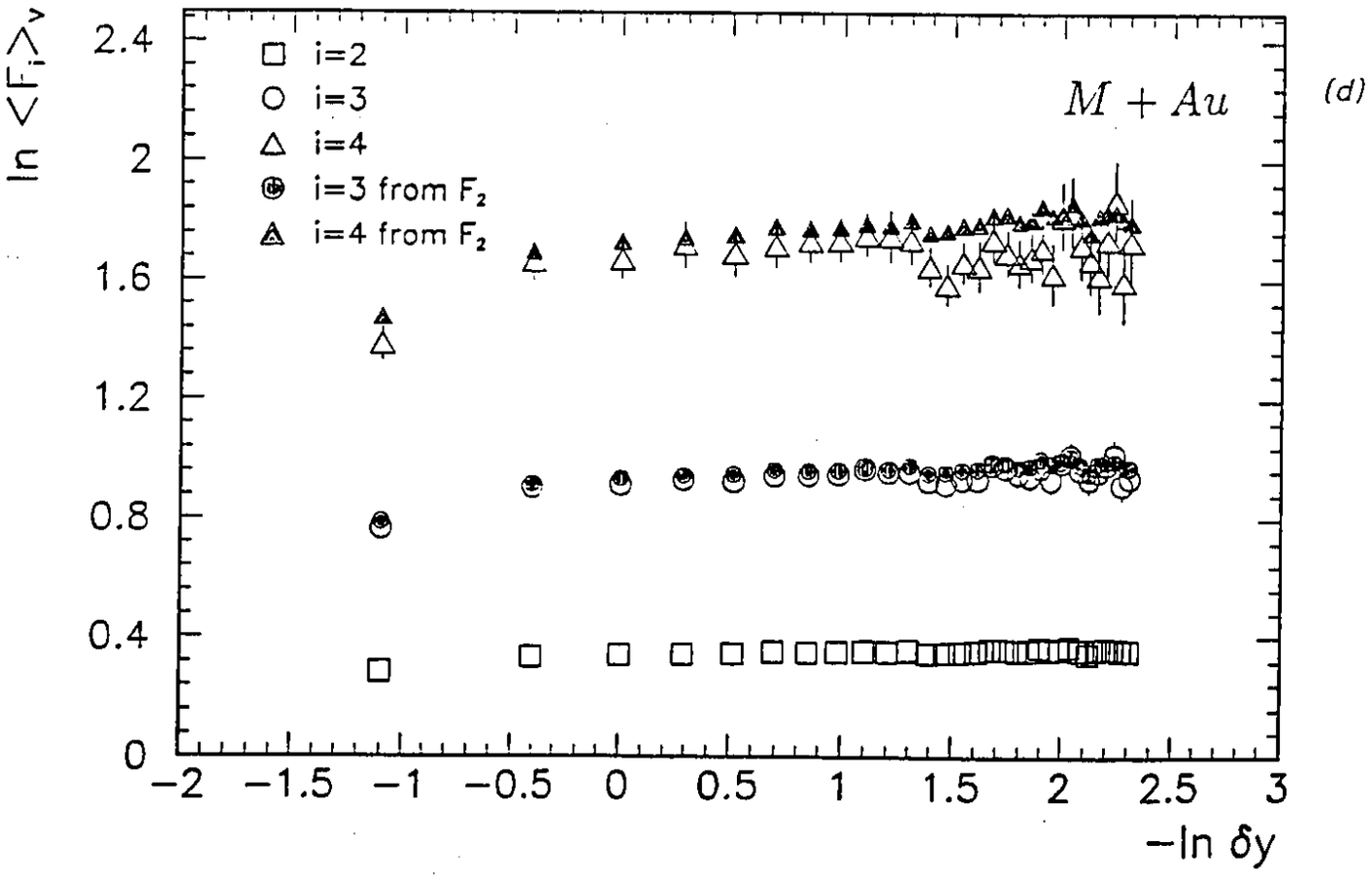
ln <F_i>_v
2.4
2
1.6
1.2
0.8
0.4
0
i=2
i=3
i=4
i=3 from F_2
i=4 from F_2
M + Au
(d)
−2
−1.5
−1
−0.5
0
0.5
1
1.5
2
2.5
3
−ln δy

Fig. 4

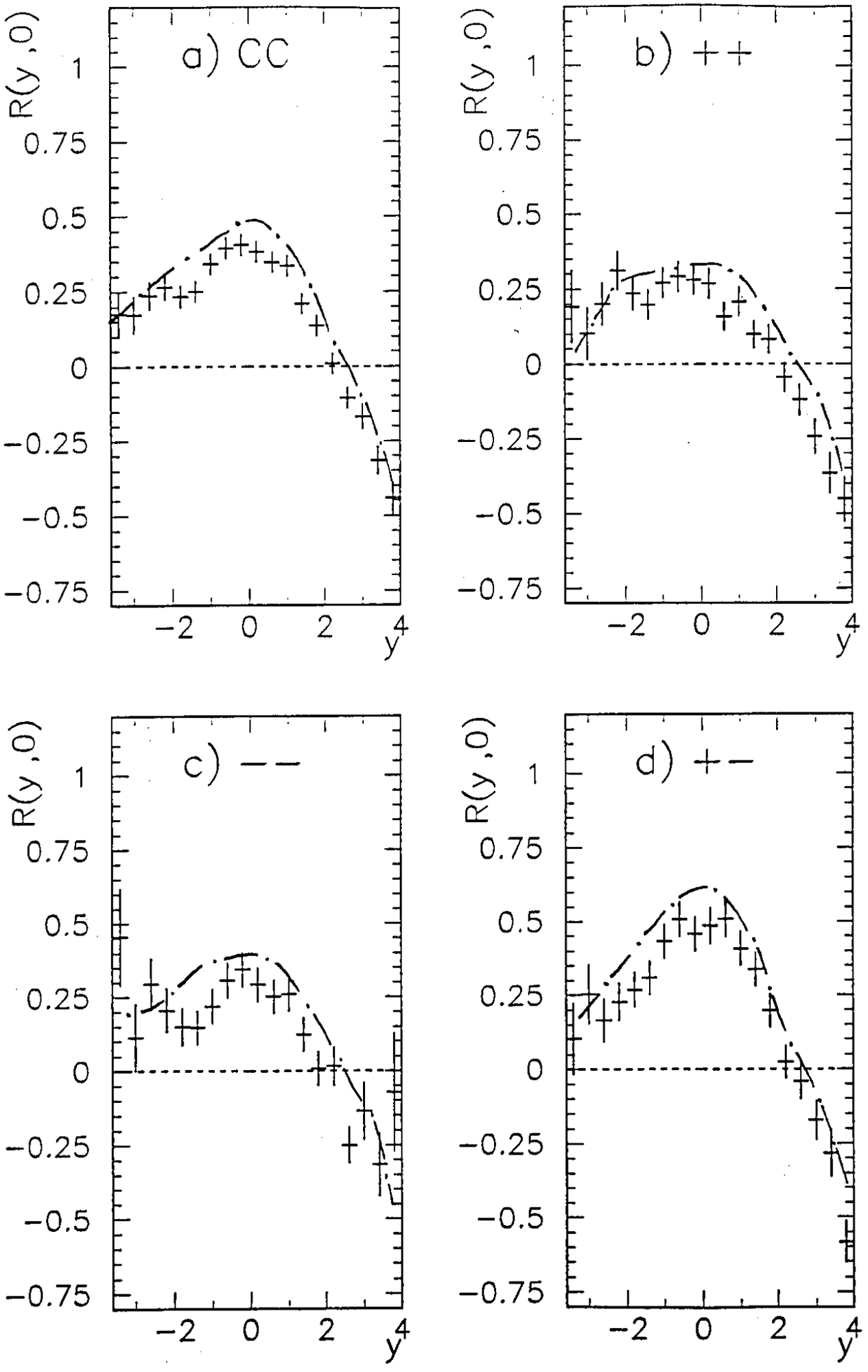

Fig. 5

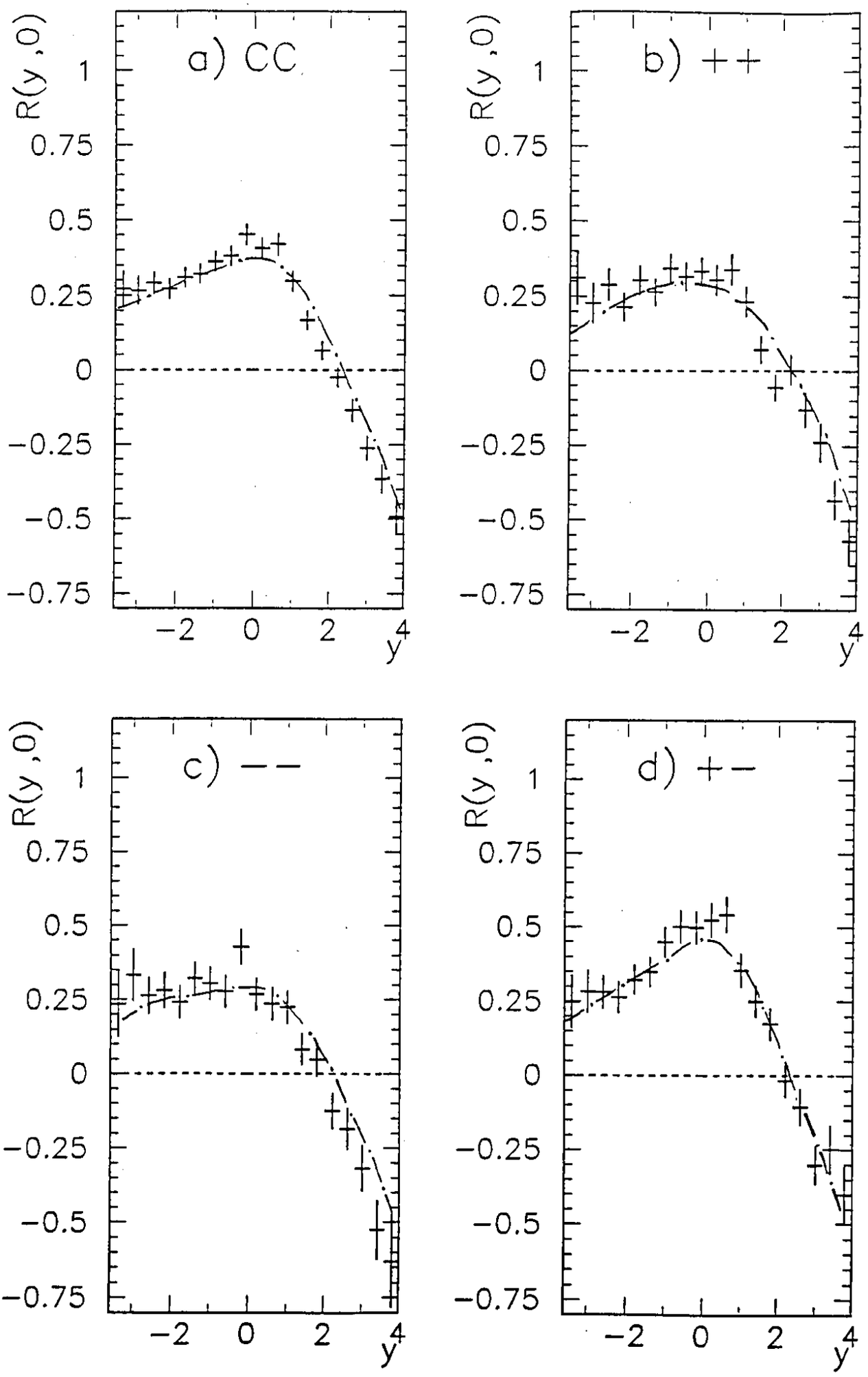

Fig. 6

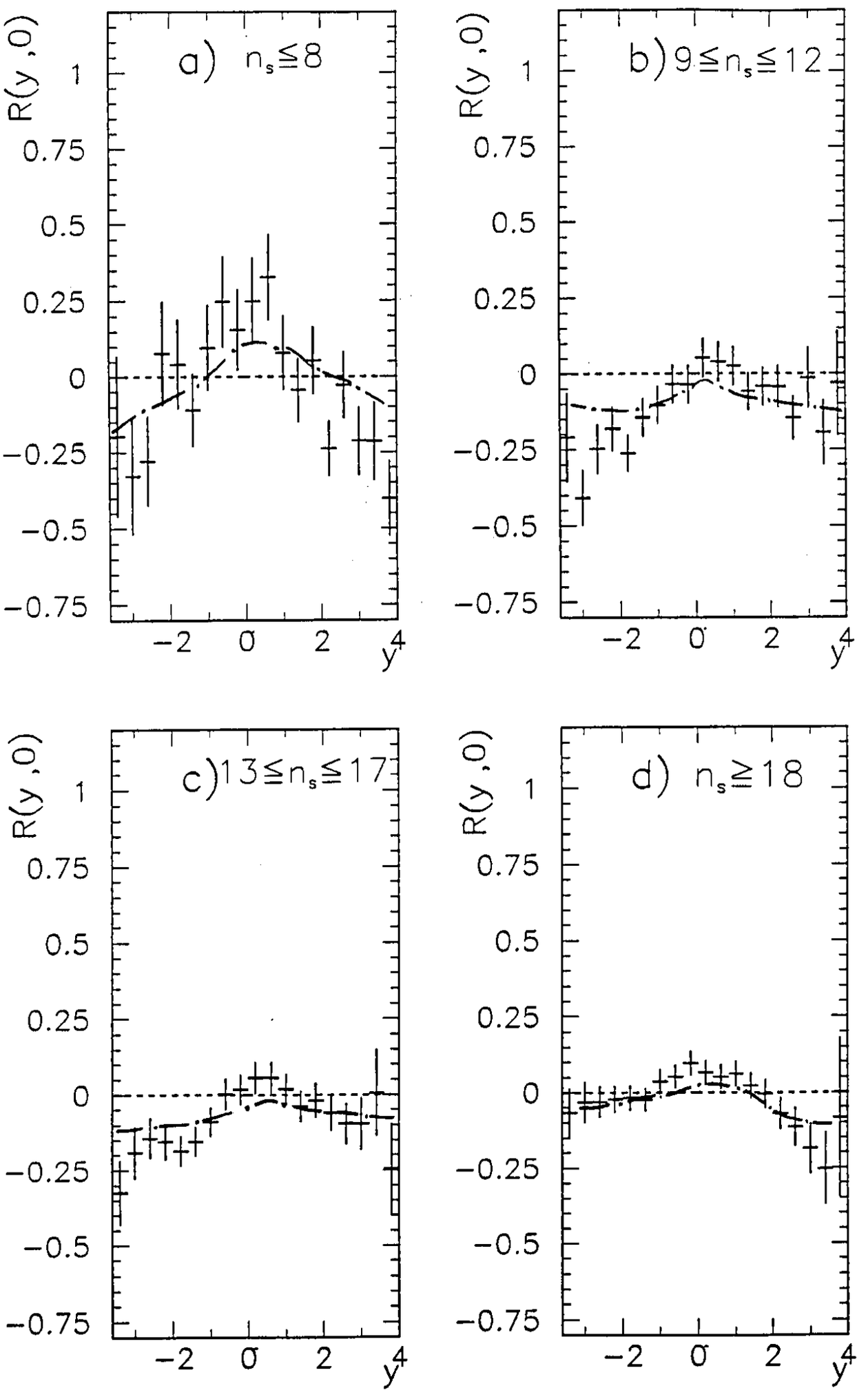
a) $n_s \leqq 8$
b) $9 \leqq n_s \leqq 12$
c) $13 \leqq n_s \leqq 17$
d) $n_s \geqq 18$
R(y,0)
y*
1
0.75
0.5
0.25
0
−0.25
−0.5
−0.75
−2
0
2
4

Fig. 7

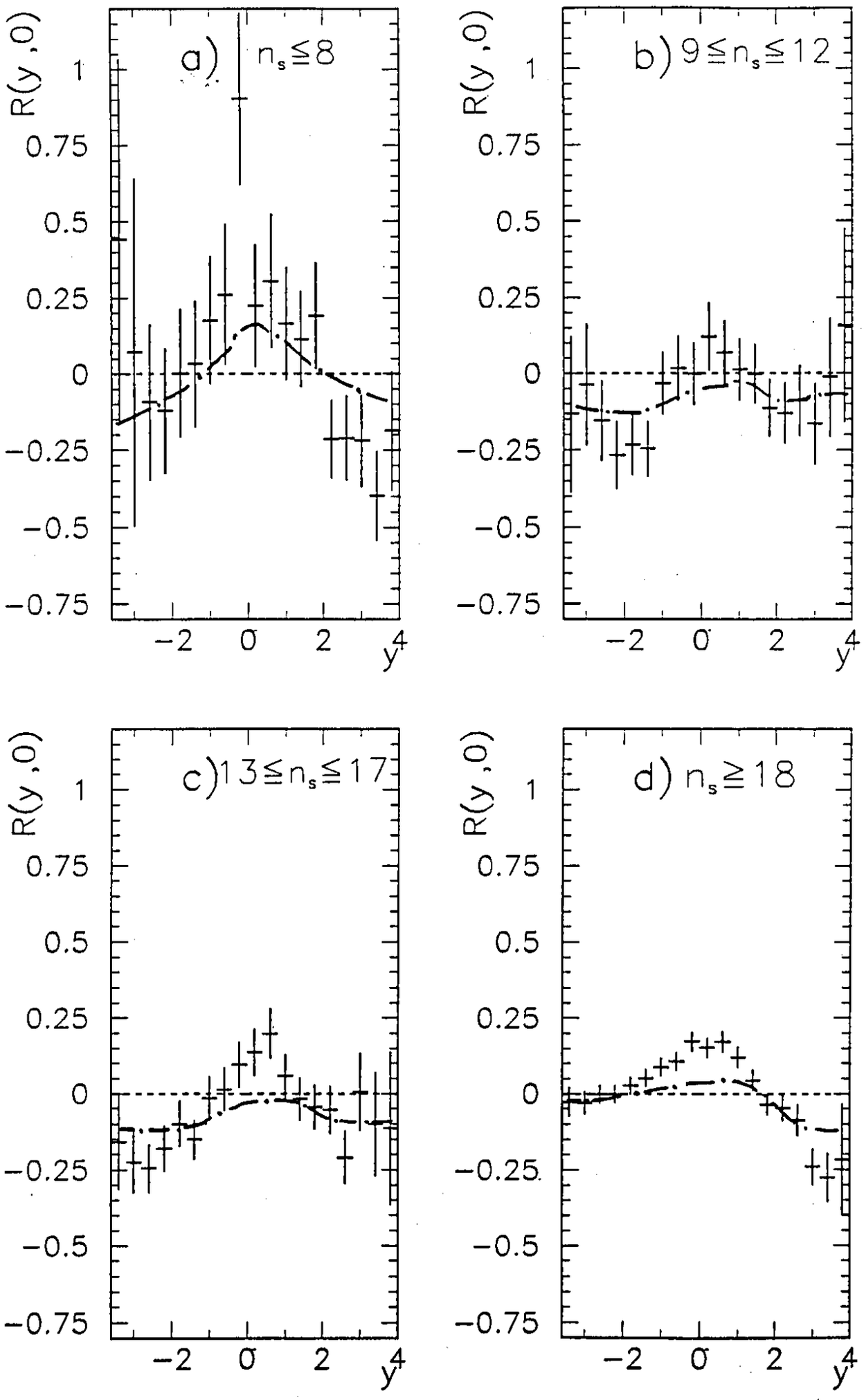
a) $n_s \leq 8$
b) $9 \leq n_s \leq 12$
c) $13 \leq n_s \leq 17$
d) $n_s \geq 18$
R(y,0)
y*
1
0.75
0.5
0.25
0
−0.25
−0.5
−0.75
−2
0
2
4

Fig. 8

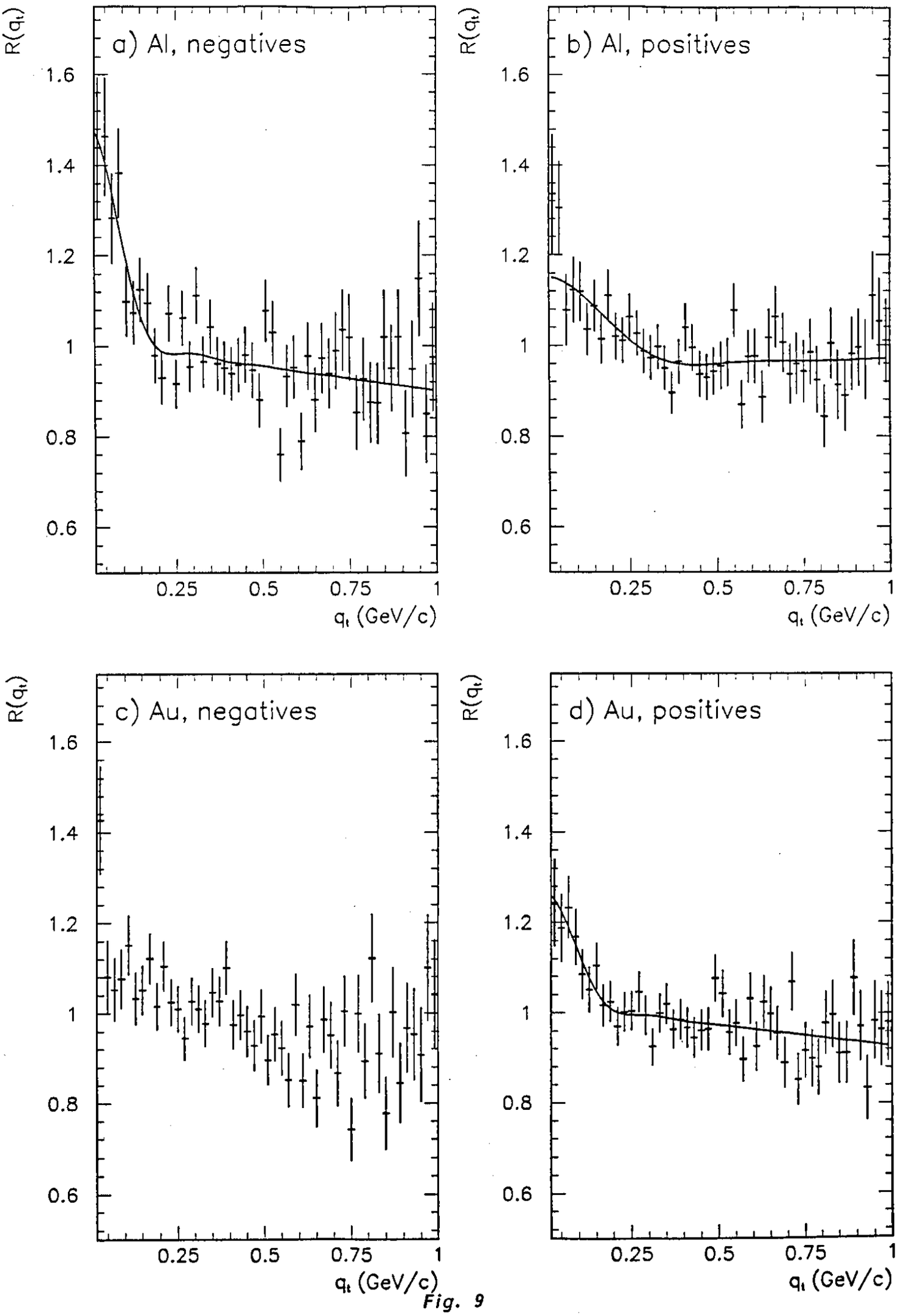
a) Al, negatives
b) Al, positives
c) Au, negatives
d) Au, positives
R(q_t)
q_t (GeV/c)
1.6
1.4
1.2
1
0.8
0.6
0.25
0.5
0.75
1

Fig. 9

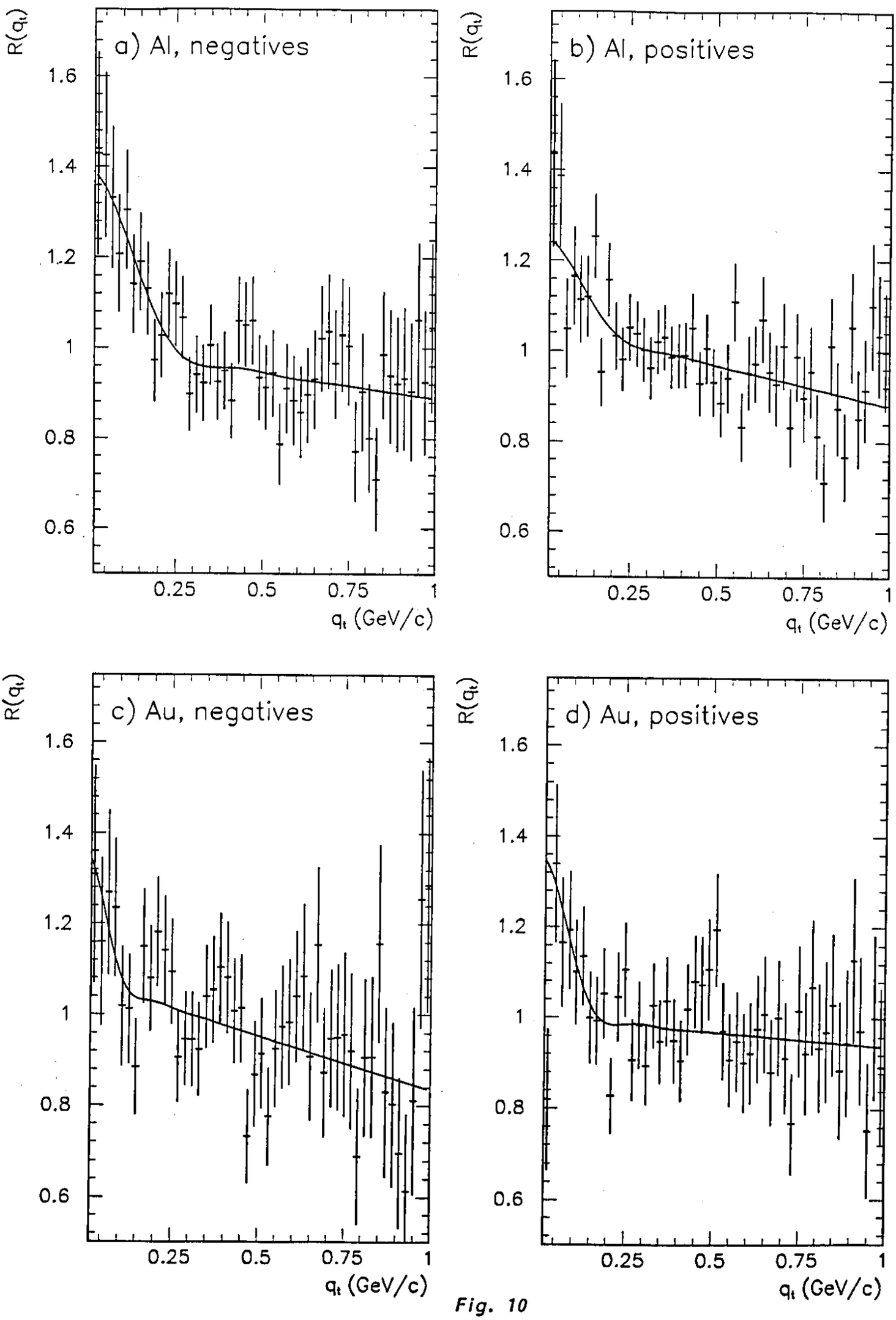
a) Al, negatives
b) Al, positives
c) Au, negatives
d) Au, positives
R(q_t)
q_t (GeV/c)
1.6
1.4
1.2
1
0.8
0.6
0.25
0.5
0.75
1

Fig. 10

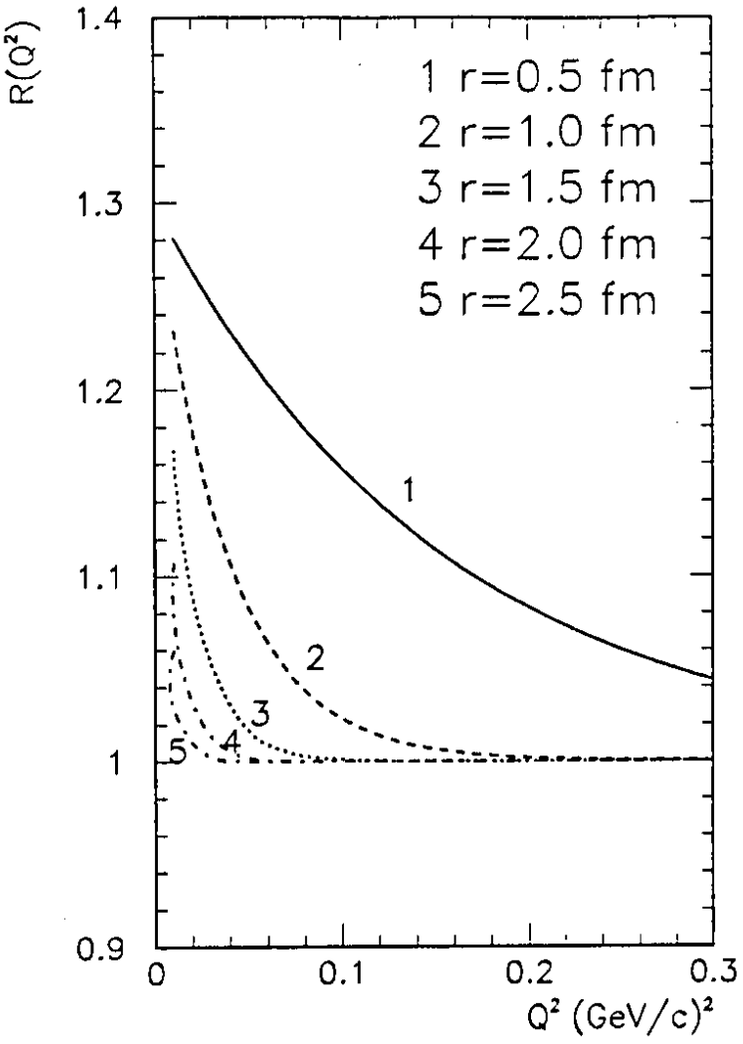
R(Q²)
1.4
1.3
1.2
1.1
1
0.9
0
0.1
0.2
0.3
Q² (GeV/c)²
1 r=0.5 fm
2 r=1.0 fm
3 r=1.5 fm
4 r=2.0 fm
5 r=2.5 fm
1
2
3
4
5

Fig. 11

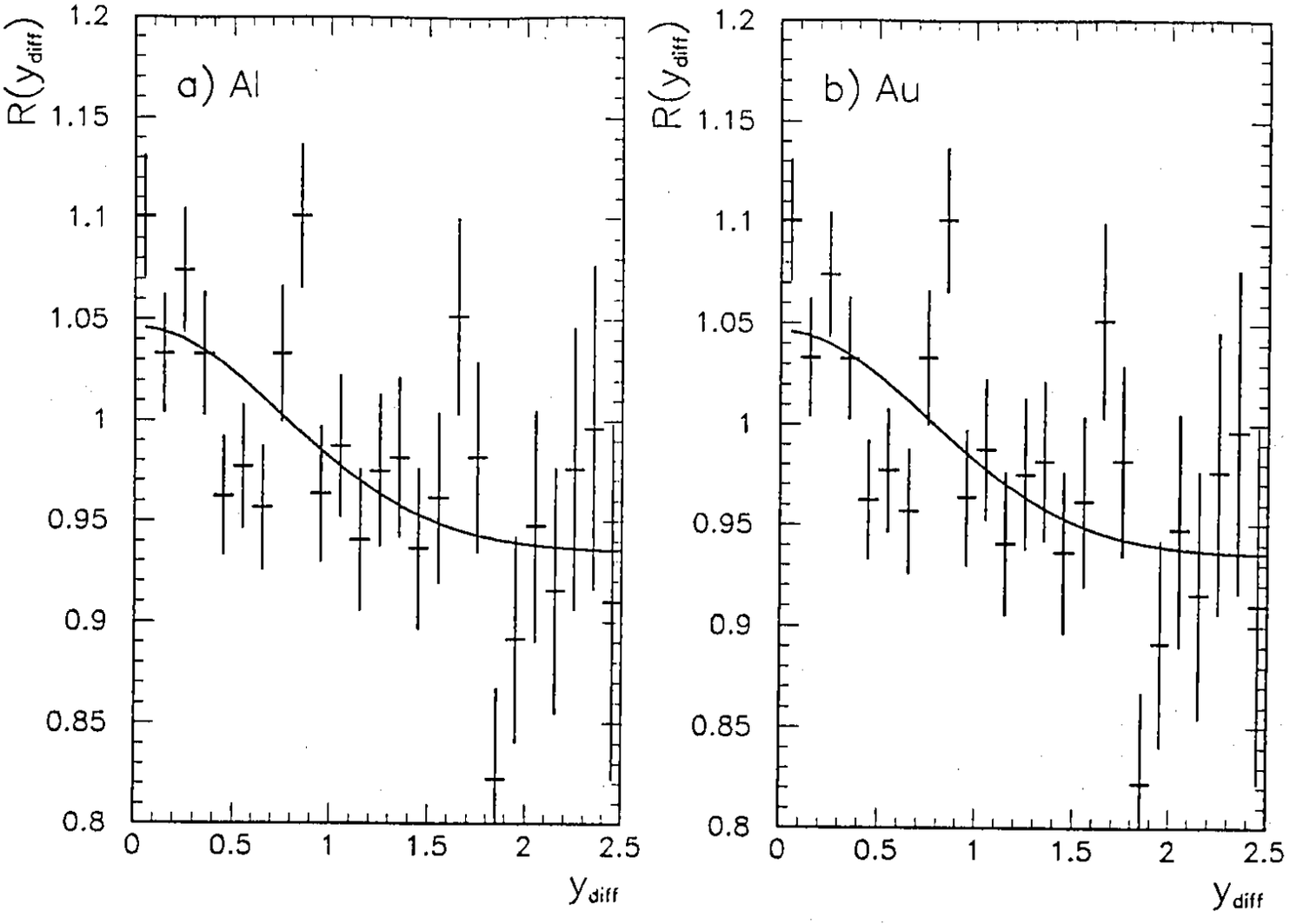

Fig. 12